A *Recql5* mutant enables complex chromosomal engineering of mouse zygotes

Satoru Iwata[1, 2, 3, 4, #], Miki Nagahara [1], Takashi Iwamoto [1, 2]

[1]Center for Education in Laboratory Animal Research, Chubu University

[2]Department of Biomedical Sciences, College of Life and Health Sciences, Chubu University

[3]College of Bioscience and Biotechnology, Chubu University

[4]Center for Mathematical Science and Artificial Intelligence, Chubu University

[#]To whom correspondence should be addressed: satoru_iwata@isc.chubu.ac.jp

Abstract

Complex chromosomal rearrangements (CCRs) are often observed in clinical samples from patients with cancer and congenital diseases but are difficult to induce experimentally. For generating animal models, these CCRs must be induced as desired, because they can generate profound genome instability and/or result in cell death. This is the first study to present the establishment of an animal model for CCRs. The disruption of *Recql5*, which degrades RAD51 during DNA repair, successfully induces CRISPR/Cas9-mediated CCRs, establishing a mouse model containing triple fusion genes and megabase-sized inversions. Notably, some of these structural features of individual chromosome rearrangements use template switching and microhomology-mediated break-induced replication mechanisms and are reminiscent of the newly described phenomenon 'chromoanasynthesis'. Whole-genome sequencing (WGS) analysis revealed that the structural variants in these mice caused only target-specific rearrangements but not target-independent complex ones. Thus, these data demonstrate that CCRs can be efficiently induced by manipulating DNA repair pathways.

Introduction

Recent advances in bioinformatics technologies have led to the detection of complex chromosome rearrangements (CCRs) consisting of ≥3 chromosomal breaks in patients with cancer and congenital diseases[1]. These rearrangements caused by catastrophic cellular events can affect phenotype, thereby inducing a disease-promoting environment[2]. In particular, chromoanasynthesis, a recently discovered form of CCRs, is caused by erroneous DNA replication of a single chromosome through fork stalling and template switching (FoSTeS) and microhomology-mediated break-induced replication (MMBIR), which generates regions of complex rearrangements[3]. However, the pathogenic mechanisms underlying these diseases remain unclarified, and the establishment of appropriate animal models is essential for their elucidation. Although recent technologies, such as clustered regularly interspaced short palindromic repeats (CRISPR)-dependent base editing, prime editing, and DNA integration, have allowed for high-precision genome interrogation[4], they have not yet been adapted to model CCRs in the germ line. Not surprisingly, the efficient and precise induction of specific chromosomal rearrangements in the laboratory is difficult and requires complex manipulation of germline systems.

Here, we hypothesised that the efficient induction of CCRs could be achieved by manipulating the DNA repair pathway as accumulating evidence indicates that changes in DNA repair timing often accompany genomic rearrangements[2]. However, given the importance of DNA repair genes in genome maintenance, these strategies may have adverse consequences. Indeed, most genes involved in the DNA repair pathway are essential, and their homozygous disruption leads to embryonic lethality in mice[5]. RecQ protein-like 5 (RECQL5) helicases can displace the DNA repair protein RAD51 from single-stranded (ss)DNA and disassemble nucleoprotein filaments, thereby suppressing homology-directed repair (HDR)[6]. Transient accumulation of the homologous recombination and RAD51 has been reported in *Recql5*-deficient cells, which could alter DNA repair pathways, thereby contributing to the chromosomal rearrangements[6]. Notably, *Recql5*-deficient mice were reported to live to adulthood[6]. Hence, we investigated whether CCRs might be induced in *Recql5*-deficient mice and successfully obtained a mouse strain containing triple fusion genes and megabase-sized inversions. The ability to induce CCRs in mouse germ cells using CRISPR/Cas9 represents a

significant step forward in genome editing technology and has the potential to impact both basic research and the development of new therapies for human disease.

Results and Discussion

Recql5 mutant enables CRISPR/Cas9-mediated CCRs in mouse zygotes

Using a previously developed *in vivo* electroporation technique, called improved genome editing via oviductal nucleic acid delivery (*i*-GONAD)[7], we first established a mouse strain with a deletion of the RAD51-binding domain in RECQL5 (*Recql5*^{em1Cu}). These *Recql5*$^{em1Cu/em1Cu}$ mice were fertile and unexpectedly showed no overt signs of other diseases such as tumorigenesis or inflammatory diseases; five male and four female mice were observed for over 60 weeks (Supplementary Fig. 1).

To generate CCRs, we selected an approximately 1.1 Mb region of mouse chromosome 10 containing *Hmga2*, *Wif1*, and *Rassf3* (Fig. 1a). These three genes are involved in human cancer and are mapped in a similar configuration in human chromosome 12. The *HMGA2–WIF1* fusion gene is involved in the Wnt/β-catenin pathway and has been found in salivary gland tumours and breast adenomyoepitheliomas[8]. *RASSF3* is an important gene in p53-dependent apoptosis and functions as a tumour suppressor[9]. We designed gRNAs targeting these three genes and single-stranded oligodeoxynucleotides (ssODNs) that joined the chromosomal breakpoints, each of which had a sequence homologous to each junction point, such that two inversions were induced by the HDR process between the targeted regions and the homologous ssODNs (Supplemental Fig. 2). The 5′ and 3′ ends of the ssODNs were protected with two consecutive phosphorothioate-modified bases to improve the HDR efficiency[10]. We then injected CRISPR/Cas9 ribonucleoproteins (RNPs) targeting *Hmga2*, *Wif1*, *Rassf3*, and ssODNs into the oviduct lumen of pregnant females on day 0.7 of pregnancy (corresponding to the late one-cell stage) and electroporated the oviduct *in vivo* (Supplemental Fig. 3). This method bypasses the following steps: (1) zygote isolation, (2) microinjection, and (3) zygote transfer[7]. The generation of predicted chromosomal rearrangements was first confirmed by PCR of genomic DNA and then validated by sequencing the corresponding fusion transcript. Here, founder (F0) mice, in which a central breakpoint was detected, were defined as having induced CCRs and were used for subsequent analyses.

In the *Recql5*$^{em1Cu/em1Cu}$ strain, we obtained six F0 pups via caesarean section and found that four had chromosomal rearrangements in the target locus, yielding three viable F0 CCRs mice (Fig. 1b, c: #1, #4a, #4b). By contrast, control WT (C57BL/6N) strains showed partial chromosomal rearrangements in three of the eight pups; however, we could not obtain the surviving founder, F0 (Fig. 1c). Despite this seemingly difficult chromosomal rearrangement pattern, we confirmed the expression of the corresponding fusion transcript using reverse transcription (RT)-PCR and direct sequencing (Fig. 1b). Homozygous *CCRs(10)*$^{\#4a}$ mice, in which all three fusion genes resulted in a recessive pygmy phenotype due to the *Hmga2* mutation[11], including severe growth retardation and infertility, did not develop tumours within the timeframe of analysis (Fig. 1d–g). These findings suggest that the Hmga2–Wif1 fusion protein expression does not play a crucial pathogenic role in mice, although observations over a prolonged period are required to assess this possibility. The mating of heterozygous *CCRs(10)*$^{\#4a}$ mice resulted in homozygous, heterozygous, and WT mice born with the expected Mendelian inheritance (Fig. 1h). Imprecise repair of double strand breaks (DSBs) has the potential to be highly deleterious owing to genomic instability, including the formation of chromosomal rearrangements[12]. Thus, this study is the first to report experimental techniques that successfully induced CCRs in the germlines of multicellular organisms.

Evaluation of genome-wide target specificity in the *Recql5* mutant

We characterised the genome structure of the mouse strains in detail using whole-genome sequencing (WGS). The *CCRs(10)*$^{\#4a}$ strain showed multiple breakpoint junctions and was classified as deletion (red), duplication (green), and tandem inversion (teal and blue) based on paired-ends with read depth changes (Fig. 2a, b). Sequencing of the breakpoint revealed microhomology patterns and sister chromatid-containing templates, in which the added insertion was dependent on the Cas9 target site (Fig. 2c). Notably, microhomologies seemed to be used to switch the nearby template during DSB repair stalling and collapse—a process termed 'fork stalling and template switching' (FoSTeS) and 'microhomology-mediated break-induced replication' (MMBIR)[13]. This structural feature of individual chromosomes is reminiscent of the newly described phenomenon 'chromoanasynthesis', which is observed in tumours, as well as in patients with congenital diseases[3]. In addition to FoSTeS/MMBIR and tandem inversions, a 601-

kb deletion was identified in the C*CRs(10)*$^{\#1}$ strain (Supplementary Fig. 4a–c). Consistent with this result, the C*CRs(10)*$^{\#1}$ strain did not express the fusion transcript corresponding to the middle of *Hmga2–Rassf3,* and no homozygotes were found (Fig. 1b, Supplementary Fig. 4e, f). The *CCRs(10)*$^{\#4b}$ genome contained a 1,016-kb duplication harbouring *Wif1* and *Rassf3* (Supplementary Fig. 5a–c). No discernible differences in phenotype were observed between the *CCRs(10)*$^{\#4b}$ and WT strains (Supplementary Fig. 5e, f).

By contrast, HDR appeared to repair two of the five breakpoints examined in the WT background, while the others were likely repaired by microhomology-mediated end joining or non-homologous end joining; however, no FoSTeS/MMBIR was observed (Supplementary Fig. 6). A previous study demonstrated that complex genome architecture confuses the DNA repair machinery and induces template-switching events driven by FoSTeS and MMBIR[2]. Thus, if the RAD51-filament is retained, loss of *Recql5* function may promote DNA repair machinery confusion and dictate the choice between the FoSTeS/MMBIR pathways.

These candidate rearrangement breakpoints were identified from WGS data using the Manta structural variation detection algorithm; however, no target-independent complex rearrangements were identified by comparing the test genomes[14] (Fig. 2d, Supplementary Fig. 4d, 5d). Thus, these results establish the efficiency and specificity of chromosomal engineering using the proposed approach.

Recql5 **mutant mediates a broad pattern of chromosomal rearrangements**

To test the broad applicability of the *Recql5* mutant approach, we generated CCRs on chromosome 2, which included topologically associating domains at the HoxD loci. These loci are necessary for the development of the proximal part of the limb, including the future arm and forearm[15]. To study the effects of the structural variants, we engineered CCRs composed of sequential inversions between *Atf2* neighbourhood (*Atf2N*) and *Hoxd1N,* and between *Hoxd1N* and *Nfe2l2N* (Fig. 3a). In the *Recql5*$^{em1Cu/em1Cu}$ strains, we screened F0 mice using PCR amplification and DNA sequencing of three junction points and detected chromosomal rearrangements in two of the four F0 mice (Fig. 3b, d). In one of the possible CCRs mouse lines, named F0-#2, two HDR-repaired junction points were detected, whereas the other junction point was

repaired with structural changes that could not be amplified by PCR (Fig. 3b). By contrast, the control C57BL/6N strain did not show any breakpoints in the five pups (Fig. 3d). Although the RNP-based CRISPR-Cas system is characterised by high-efficiency germline transmission[16], F0-#2 did not transmit the targeted CCRs to their 34 offspring. In additional studies, we examined DNA extracted from the testes and semen of F0-#2 animals; however, the semen samples did not exhibit a PCR signal (Fig. 3c). In our experience, F0-#2 was the first mouse line in which the mutation was not transmitted to the gametes using an RNP-based CRISPR-Cas system. Asymmetric disjunction results in a wide range of highly imbalanced gametes, many of which do not survive until the end of spermatogenesis[17]. Breakpoints in intergenic regions may disturb the interactions between the promoter and transcriptional units with its *cis*-acting regulators through positional effects, thus severely affecting gene expression[18].

We recently succeeded in inducing a 7.67 Mb inversion in WT mice[19] (Supplementary Fig. 7a). We induced this large inversion in the *Recql5*$^{em1Cu/em1Cu}$ mice as well, with higher genome editing efficiency than that in WT mice (Supplementary Fig. 7b, h). Homozygous inversion mice, named *In(15)*$^{\#6}$, exhibited a white-spotted phenotype due to the disrupted *Adamts20*, were generated by breeding heterozygous males and females (Supplementary Fig. 7f).

Next, we efficiently modelled the *Hmga2–Wif1* inversion on chromosome 10 in *Recql5*$^{em1Cu/em1Cu}$ mice, as shown in Fig. 1 (Supplementary Fig. 7c). The resulting mice, named *In(10)*$^{\#2}$, invariably harboured the *Hmga2–Wif1* inversion, expressed the *Hmga2–Wif1* fusion gene, and displayed a recessive pygmy phenotype due to the *Hmga2* mutation[11] (Supplementary Fig. 7d, e, g, h).

Upon closer inspection of the repaired regions in the inversions of the two mice (*In(15)*$^{\#6}$, *In(10)*$^{\#2}$) obtained using *Recql5* mutants, we found that both mice harboured a complete ssODN sequence at the breakpoint (Supplementary Fig. 7b, d). Thus, the structural features of induced rearrangements are likely to depend on a variety of factors, such as features specific to the targeted genomic regions, the number of breakpoints, and the unique properties of the mouse lines.

Conclusions

Here, we describe a new genome editing method using a *Recql5* mutant mouse and show that it can efficiently induce various types of chromosomal rearrangements, including CCRs and inversions, in mouse zygotes. To the best of our knowledge, this is the first study to successfully introduce CCRs into mouse zygotes using CRISPR-based methods. Although this technique has great potential, it is also associated with unexpected DSB repair mechanisms such as FoSTeS/MMBIR. In FoSTeS and MMBIR models, the absence of a homologous template during HDR results in the activation of microhomology pairing repair of broken ends, a more error-prone DNA repair. Thus, these factors need to be carefully considered during the application of such techniques to therapeutics. This approach opens new avenues for investigating the role of chromosomal rearrangements in diseases and provides a powerful tool for engineering genetic modifications in various organisms. However, further studies are required to optimise the efficiency and specificity of this approach and explore its potential for therapeutic applications.

Methods

Animal strains

C57BL/6NCrSlc mice (Japan SLC, Shizuoka, Japan) were used in this study. The animals were housed at a constant temperature (22 ± 2 °C) and humidity (50 ± 10%), with a 12-h light/12-h dark cycle. All animal experiments were approved by the Institutional Animal Care and Use Committee of Chubu University (Permit Number #202110033) and were conducted in accordance with institutional guidelines.

CRISPR RNP and ssODN preparation

The CRISPR guide RNAs were designed using CHOPCHOP[20] (http://chopchop.cbu.uib.no/) (Supplementary Table 1). CRISPR RNP consists of Alt-R S.p. Cas9 Nuclease 3NLS (Integrated DNA Technologies, Coralville, IA, USA) and a custom guide RNA (crRNA): universal structural RNA (tracrRNA) duplex (Integrated DNA Technologies). crRNA and tracrRNA were heated to 95 °C for 10 min and slowly cooled to 25 °C. This crRNA:tracrRNA duplex and the Alt-R S.p. Cas9 Nuclease 3NLS were incubated at 25 °C for 10 min to form the RNP complex. The ssODNs were manufactured by Eurofins Genomics (Tokyo, Japan) and were designed to join two DNA sequences so that the junction would be positioned at the centre of the predicted cleavage sites, which were located within 3 bp of the PAM sequences (Supplementary Table 2). The 5′ and 3′ ends of the ssODNs were protected with two consecutive phosphorothioate-modified bases to improve the HDR efficiency[10].

i-GONAD method

C57BL/6NCrSlc female mice (8–12 weeks old) in oestrus were mated with males (8–24 weeks old) at 15:00–18:00 h. The presence of copulation plugs was confirmed the next morning via visual inspection, and plug-positive mice were subjected to *i*-GONAD experiments, as previously described[7]. The following CRISPR solutions were used: 540 ng/μL Alt-R S.p. Cas9 Nuclease 3NLS, 33 μM upstream and downstream crRNA:tracrRNA, and 0.05% Fast Green FCF (Wako, Osaka, Japan) marker diluted in Opti-MEM (Thermo Fisher Scientific, Waltham, MA, USA). Prior to electroporation, females were anaesthetised with a mixture of medetomidine (0.75 mg/kg), midazolam (4 mg/kg), and butorphanol (5 mg/kg). The CRISPR mixture (1 μL) was injected into

the oviductal lumen upstream of the ampulla using a glass micropipette including a vertical capillary puller (NARISHIGE, Tokyo, Japan). The CRISPR mixture was injected using a FemtoJet 4i microinjector (Eppendorf, Hamburg, Germany) with the following settings: pi: 100 hPa, ti: 0.2 s, and pc: 0 hPa. After injection of CRISPR solutions, the oviduct regions were clamped using tweezer electrodes (LF650P3; BEX, Tokyo, Japan), and electroporation was performed as previously described[16, 17] using a CUY21EDIT II (BEX, Tokyo, Japan). The following parameters were used for electroporation: square (mA), (+/−), Pd V: 60 V or 80 V, Pd A: 200 mA, Pd on: 5.00 ms, Pd off: 50 ms, Pd N: 3, Decay: 10%, DecayType: Log. Thereafter, we placed the oviducts back in their original location and sutured the incisions. Post operation, atipamezole hydrochloride (0.75 mg/kg) was intraperitoneally injected to reverse the effects of medetomidine.

Analysis of CRISPR/Cas9-engineered mice

To screen for CRISPR/Cas9-induced mutations, genomic DNA was isolated from the tails or ears of founder mice using lysis buffer [100 mM NaCl, 200 mM sucrose, 10 mM ethylenediaminetetraacetic acid, 300 mM Tris (pH 8.0), and 1% sodium dodecyl sulfate], and DNA was examined by PCR amplification. The obtained PCR products were purified using NucleoSpin Gel and PCR Cleanup kit (Takara Bio, Shiga, Japan) and sequenced directly or were cloned into the pTAC-1 vector (Biodynamics, Tokyo, Japan), and the sequences of individual clones were determined using Sanger sequencing (Eurofins Genomics, Tokyo, Japan). The PCR primers used for genotyping are listed in Supplementary Table 3.

RT-PCR

Reverse transcriptase (RT)-PCR was performed using total RNA. Total RNA was isolated from ear tissue using ISOSPIN Cell & Tissue RNA (Nippon Gene, Tokyo, Japan). Template cDNA was obtained using ReverTra Ace qPCR RT Master Mix (Toyobo, Osaka, Japan). The RT-PCR products were treated with NucleoSpin Gel and PCR Cleanup kit (Takara Bio, Shiga, Japan) and directly analysed using Sanger sequencing (Eurofins Genomics, Tokyo, Japan). The primers used for RT-PCR are listed in Supplementary Table 3.

Growth analysis

From 0 to 12 weeks after birth, the weight (g) of *CCRs(10)*$^{\#4a/\#4a}$, *CCRs(10)*$^{\#4a/+}$, and WT (+/+) mice was recorded for growth curve analysis.

Food intake analysis

Mice were housed individually, and food intake was measured in terms of grams of diet consumed per day.

Mating test

Upon sexual maturation, male mice were caged with two females for at least 8 weeks. During the mating test, pups were counted for litter size measurements and their tails or ears were biopsied for genotyping.

Whole-genome sequencing analysis

Total genomic DNA was extracted using a DNeasy Blood & Tissue Kit (Qiagen, Hilden, Germany). The library was prepared using TruSeq Nano DNA (Illumina, CA, USA) according to the manufacturer's library quantification protocol. Sequencing was performed as pair-end (150 bp) using an Illumina NovaSeq6000 (Illumina) by Macrogen sequencing service (Macrogen Inc., Seoul, Korea). Whole-genome sequencing analysis and genomic coordinates provided in this manuscript are based on the GRCm38/mm10 assembly. The sequencing data were then aligned in BAM format to the mouse reference genome (mm10) using the Integrative Genomics Viewer (IGV-version 2.3.93). Structural rearrangements and breakpoints were identified using Manta Structural Variant Caller[14] (version 1.3.1). Breakpoints were visually inspected using IGV (IGV-version 2.3.93) to confirm the presence of split and spanning reads.

Statistical analysis

The Student's *t*-test (two-tailed test) was used for body weight, food intake, and mating analyses. Data are presented as mean ± standard deviation (SD). For Mendelian genotype ratios of progeny obtained from sibling mating between CCRs mice, the chi-square test was performed using Excel version 16.36 (Microsoft, Redmond, WA, USA).

Statistical comparisons were made using Tukey's Honestly Significant Differences (Tukey's HSD) test. The threshold for statistical significance was $P < 0.05$.

Acknowledgements

The authors thank the laboratory members for their support with animal care and experiments. This study was supported by JSPS KAKENHI for a Grant-in-Aid for Scientific Research (B) (to S.I., Grant Number 21H02395) and The Science Research Promotion Fund 2022 (to S.I., Grant Number 29).

Contributions

S.I. designed and performed the experiments and drafted the manuscript. M.N. performed the animal experiments. T.I. supervised the studies and corrected the manuscript. All authors have read and approved the final manuscript.

Competing interests

The authors declare no competing interests.

References

1. Pellestor, F. Chromoanagenesis: cataclysms behind complex chromosomal rearrangements. *Mol. Cytogenet.* 12, 6 (2019).
2. Burssed, B. et al. Mechanisms of structural chromosomal rearrangement formation. *Mol. Cytogenet.* 15, 23 (2022).
3. Pellestor, F. & Gatinois, V. Chromoanasynthesis: another way for the formation of complex chromosomal abnormalities in human reproduction. *Hum. Reprod.* 33, 1381–1387 (2018).
4. Nambiar, T. S. et al. CRISPR-based genome editing through the lens of DNA repair. *Mol. Cell*, 82, 348–388 (2022).
5. Menolfi, D. & Zha, S. ATM, ATR and DNA-PKcs kinases—the lessons from the mouse models: inhibition ≠ deletion. *Cell Biosci.* 10, 8 (2020).
6. Hu, Y. et al. RECQL5/Recql5 helicase regulates homologous recombination and suppresses tumor formation via disruption of Rad51 presynaptic filaments. *Genes Dev.* 21, 3073–3084 (2007).
7. Ohtsuka, M. et al. i-GONAD: a robust method for in situ germline genome engineering using CRISPR nucleases. *Genome Biol.* 19, 25 (2018).
8. Pareja, F. et al. Assessment of HMGA2 and PLAG1 rearrangements in breast adenomyoepitheliomas. *NPJ Breast Cancer* 5, 6 (2019).
9. Kudo, T. et al. The RASSF3 candidate tumor suppressor induces apoptosis and G1–S cell-cycle arrest via p53. *Cancer Res* 72, 2901–2911 (2012).
10. Renaud, J. B. et al. Improved genome editing efficiency and flexibility using modified oligonucleotides with TALEN and CRISPR-Cas9 nucleases. *Cell Rep.* 14, 2263–2272 (2016).
11. Lee, M. O. et al. Hmga2 deficiency is associated with allometric growth retardation, infertility, and behavioral abnormalities in mice. *G3 (Bethesda)* 12, jkab417 (2022).
12. Brunet, E., & Jasin, M. Induction of chromosomal translocations with CRISPR-Cas9 and other nucleases: understanding the repair mechanisms that give rise to translocations. *Adv. Exp. Med. Biol.* 1044, 15–25 (2018).
13. Lee, J. A., Carvalho, C. M. & Lupski, J. R. A DNA replication mechanism for generating nonrecurrent rearrangements associated with genomic disorders. *Cell* 131, 1235–1247 (2007).

14. Chen, X. et al. Manta: rapid detection of structural variants and indels for germline and cancer sequencing applications. *Bioinformatics* 32, 1220–1222 (2016).
15. Acemel, R. D. et al. A single three-dimensional chromatin compartment in amphioxus indicates a stepwise evolution of vertebrate Hox bimodal regulation. *Nat. Genet.* 48, 336–341 (2016).
16. Chen, S. et al. Highly efficient mouse genome editing by CRISPR ribonucleoprotein electroporation of zygotes. *J. Biol. Chem.*291, 14457–14467 (2016).
17. Li, L. et al. Familial complex chromosome rearrangement (CCR) involving 5 breakpoints on chromosomes 1, 3 and 13 in a severe oligozoospermic patient. *J. Assist. Reprod. Genet.* 30, 423–429 (2013).
18. Liang, Y. et al. Complex chromosomal rearrangement causes male azoospermia: a case report and literature review. *Front. Genet.* 13, 792539 (2022).
19. Iwata, S. et al. Simple and large-scale chromosomal engineering of mouse zygotes via in vitro and in vivo electroporation. *Sci. Rep.* 9, 14713 (2019).
20. Labun, K. et al. CHOPCHOP v3: expanding the CRISPR web toolbox beyond genome editing. *Nucleic Acids Res*. 47, W171–W174 (2019).

Figures and Figure Legends

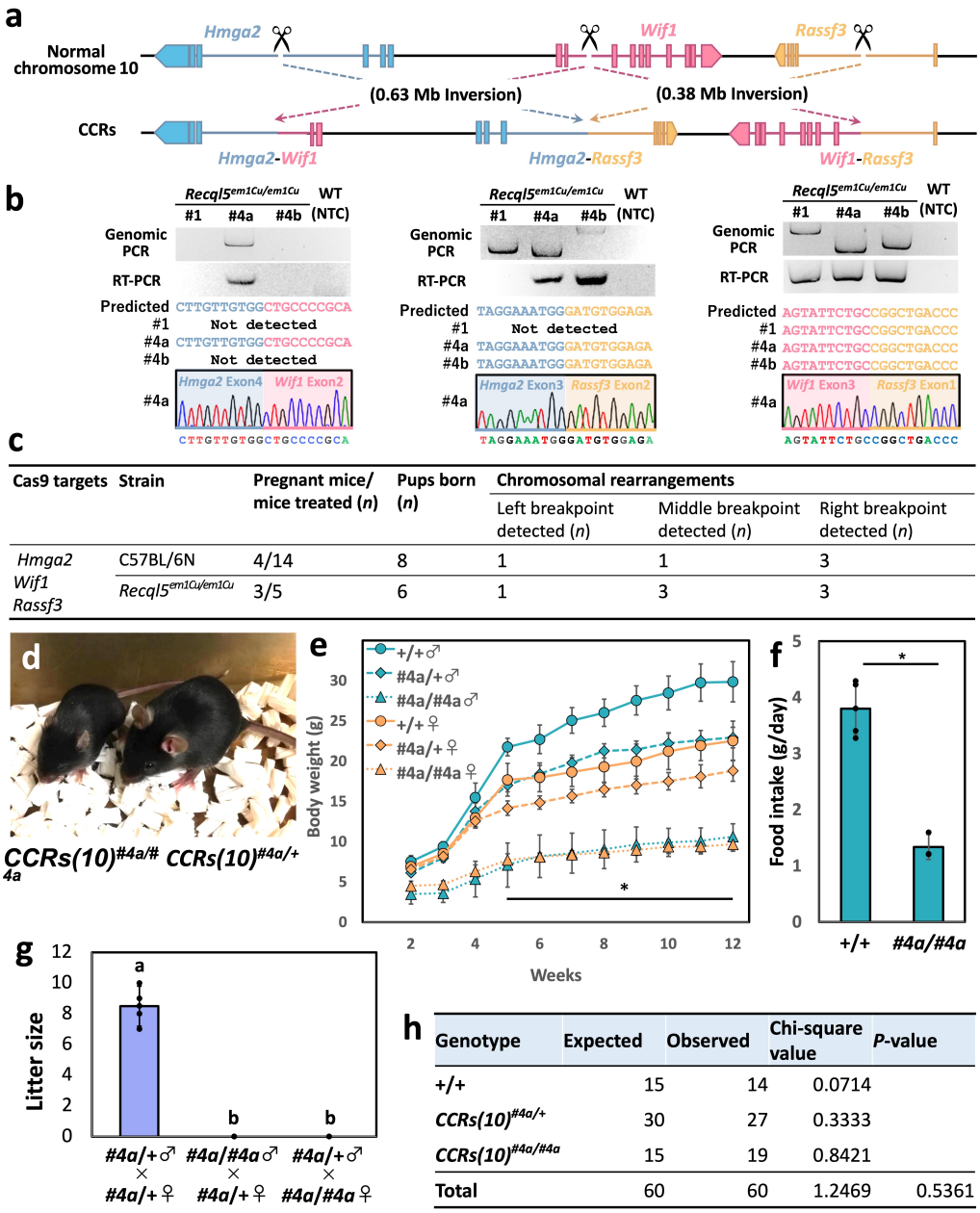

Cas9 targets	Strain	Pregnant mice/ mice treated (*n*)	Pups born (*n*)	Chromosomal rearrangements		
				Left breakpoint detected (*n*)	Middle breakpoint detected (*n*)	Right breakpoint detected (*n*)
Hmga2 *Wif1* *Rassf3*	C57BL/6N	4/14	8	1	1	3
	Recql5$^{em1Cu/em1Cu}$	3/5	6	1	3	3

Genotype	Expected	Observed	Chi-square value	*P*-value
+/+	15	14	0.0714	
CCRs(10)$^{\#4a/+}$	30	27	0.3333	
CCRs(10)$^{\#4a/\#4a}$	15	19	0.8421	
Total	60	60	1.2469	0.5361

Fig. 1: Induction of *Hmga2-Wif1*, *Hmga2-Rassf3*, and *Wif1-Rassf3* complex rearrangements in mouse zygotes using the *Recql5* mutant.

(**a**) Schematic representation of the CCRs created between *Hmga2*, *Wif1*, and *Rassf3* in chromosome 10. (**b**) PCR amplification of predicted breakpoint junction and fusion transcript. Sanger sequences corresponding to *Hmga2–Wif1*, *Hmga2–Rassf3*, and *Wif1–Rassf3* cDNA. NTC: Negative control. (**c**) Summary of the experimental efficiency of

complex chromosomal rearrangements. (**d**) Appearance of heterozygous and homozygous *CCRs(10)*$^{\#4a}$ male mice at 6 weeks of age. (**e**) Growth curves of WT (+/+) (n = 11/10), heterozygous *CCRs(10)*$^{\#4a}$ (#4a/+) (n = 7/8), and homozygous *CCRs(10)*$^{\#4a}$ (#4a/#4a) (n = 9/12) mice (female/male). Error bars, mean ± S.D. *$P < 0.05$ (two-tailed Student's *t*-test). (**f**) Food intake (g/day) of WT (+/+) and *CCRs(10)*$^{\#4a/\#4a}$ male mice (20 weeks of age). Error bars, mean ± S.D. *$P < 0.05$ (two-tailed Student's *t*-test). (**g**) Comparison of litter sizes. Error bars, mean ± S.D. (n = 6). Different letters above the bars indicate statistically significant differences at $P < 0.05$ by Tukey's HSD. (**h**) Mendelian ratios of new-born mice from *CCRs(10)*$^{\#4a}$ heterozygous crossings.

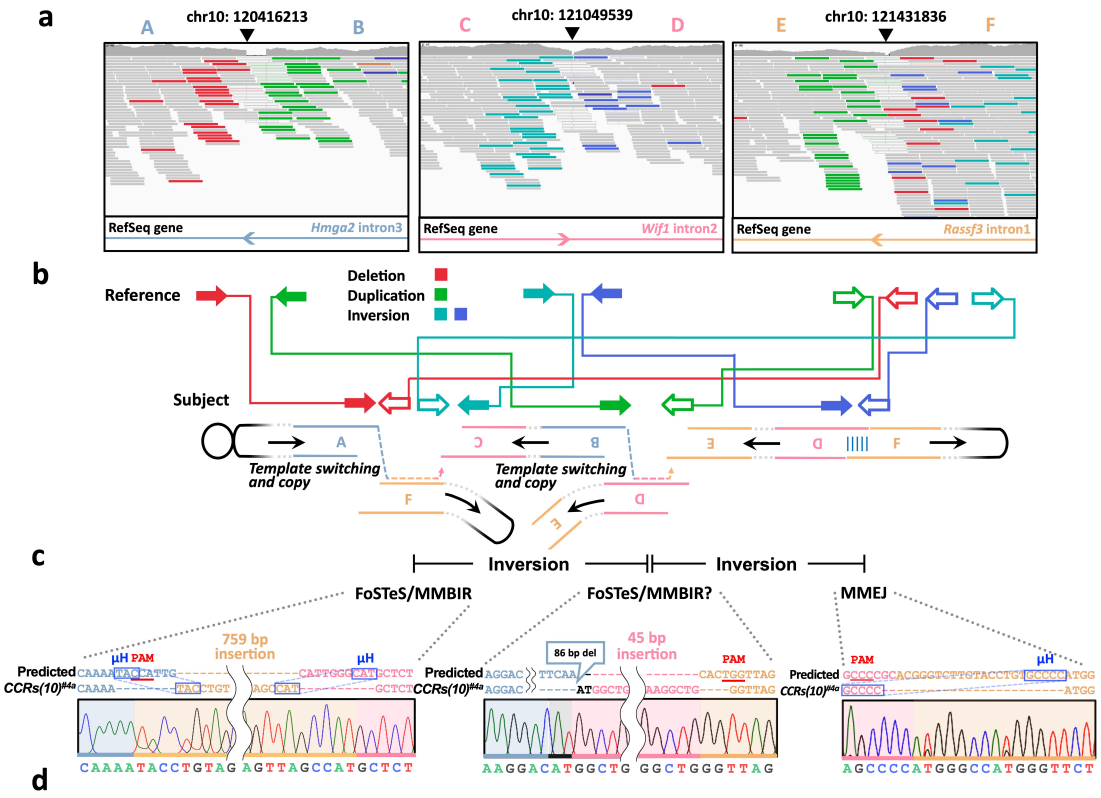

Type		#Chromo	Start	End	Size	Pair count	Quality value
Deletion		10	120416210	121431851	1015641	20	2786
Duplication		10	120416304	121431836	1015532	20	2786
Inversion		10	121049545	121432616	383071	30	1777
Inversion		10	121049558	121431864	382306	10	1777

Fig. 2: Validation of genome-wide target specificities in the *Recql5* mutant.

(**a**) Whole-genome sequencing results. Interrogative genomic viewer (IGV) browser of CCRs data aligned to the mouse genome (mm10). gRNA cut sites are shown by black arrowheads. Deleted regions are shown in red; duplicated regions are shown in green; teal and blue reads indicate that they are mapped to the reverse strand. Normal reads are shown in grey. (**b**) Schematic indicating paired-end read interpretation in IGV for complex rearrangements. Read pairs are coloured as per their interpretation in IGV. (**c**) Alignment of sequences from PCR products corresponding to the *Hmga2–Wif1*, *Hmga2–Rassf3*, and *Wif1–Rassf3* genomic breakpoint junctions. (**d**) Manta calls supporting chromosomal breakpoints.

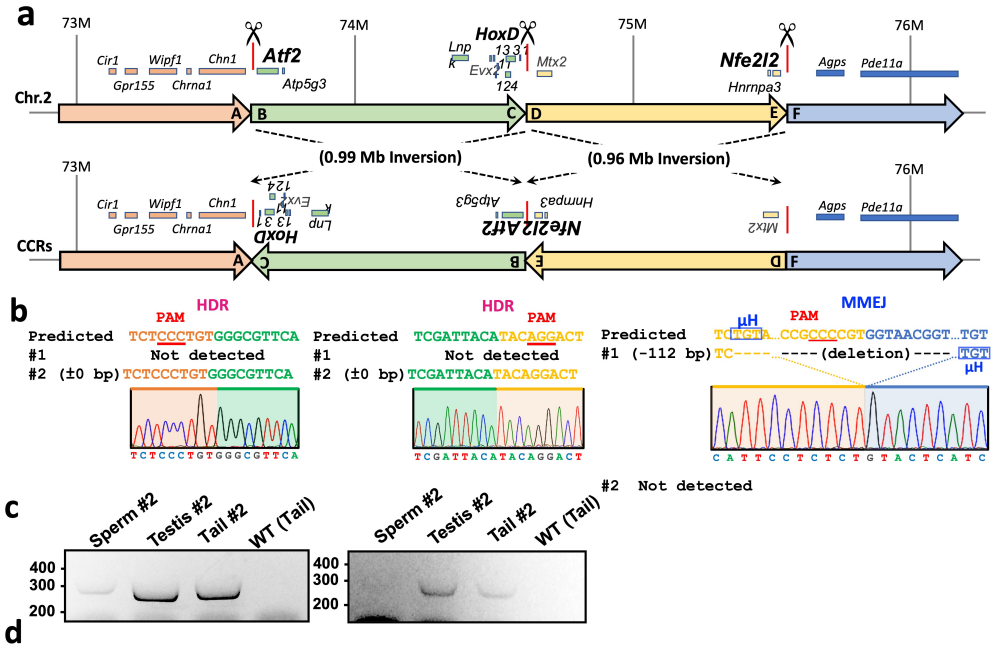

Cas9 targets	Strain	Pregnant mice/mice treated (*n*)	Pups born (*n*)	Chromosomal rearrangements		
				Left breakpoint detected (*n*)	Middle breakpoint detected (*n*)	Right breakpoint detected (*n*)
Atf2N *Hoxd1N* *Nfe2l2N*	C57BL/6N	2/9	5	0	0	0
	Recql5$^{em1Cu/em1Cu}$	2/4	4	1	1	1

Fig. 3: Complex chromosomal engineering in mouse zygotes at the HoxD loci using the *Recql5* mutant.

(**a**) Schematic of the CCRs created between the *Atf2N*, *HoxD1N*, and *Nfe2l2N* in chromosome 2. (**b**) Alignment of the sequences corresponding to the *Atf2N–HoxD1N*, *Atf2N–Nfe2l2N*, and *HoxD1N–Nfe2l2N* genomic breakpoint junctions. (**c**) PCR amplification of the breakpoint junctions in CRRs mouse sperm, testes, tail, and wild-type (WT). (**d**) Summary of the experimental efficiency of complex chromosomal rearrangements.